Crystal structure of bovine mitochondrial factor B at 0.96-Å resolution

John K. Lee*, Grigory I. Belogrudov[†‡], and Robert M. Stroud*[‡]

*Department of Biochemistry and Biophysics, University of California, San Francisco, CA 94158-2517; and [†]Department of Physiology, David Geffen School of Medicine, University of California Los Angeles, and Veterans Administration, Greater Los Angeles Healthcare System, Los Angeles, CA 90073-1003

Edited by Robert Langer, Massachusetts Institute of Technology, Cambridge, MA, and approved July 14, 2008 (received for review June 11, 2008)

Coupling factor B (FB) is a mitochondrial inner membrane polypeptide that facilitates the energy-driven catalysis of ATP synthesis in animal mitochondria by blocking a proton leak across the membrane. Here, we report the crystal structure of the bovine mitochondrial FB mutant with Gly-3–Glu substitution determined at a resolution of 0.96 Å and that of the WT polypeptide at a resolution of 2.9 Å. The structure reveals an oblong, oval-shaped molecule with a unique globular N-terminal domain that is proposed to be the membrane anchor domain and the capping region to the C-terminal leucine-rich repeats domain. A short N-terminal α-helix, which extends away from the molecule's body, is suggestive of functioning as an anchor for FB to the matrix side of the mitochondrial inner membrane. Identification of a bound Mg^{2+} ion reveals that FB is a metalloprotein. We also report the cocrystal structures of FB bound with phenylarsine oxide and Cd^{2+}, two known inhibitors of the FB coupling activity.

ATP synthase | energy coupling | leucine-rich repeat | mitochondria | x-ray crystallography

Most of the ATP in the eukaryotic cell is synthesized through oxidative phosphorylation in mitochondria (1). The bovine mitochondrial ATP synthase complex, which catalyzes the terminal step of oxidative phosphorylation, is composed of at least 16 different subunits (2). The enzyme from *Escherichia coli* has a much simpler subunit composition and is made up of eight polypeptides encoded by the *unc* operon (3). A recently characterized rat liver ATP synthasome revealed stoichiometric amounts of the ADP/ATP and phosphate carriers (4, 5) associated with ATP synthase. The animal mitochondria enzyme belongs to F-type ATPases and comprises two sectors called F_1 and F_o. The catalytic sector F_1 is a mechano-chemical transducer that synthesizes ATP under physiological conditions (6). The membrane-embedded sector F_o is a rotary motor that converts energy conserved in the proton-motive force into mechanical work (7). Both sectors are connected through the central (part of rotor) and peripheral (part of stator) stalks.

Mitochondrial coupling factor B (FB) restores oxidative phosphorylation and partial energy-driven reactions in "nonphosphorylating" membrane vesicles prepared from heavy bovine heart mitochondria (2, 8–12). Since its discovery by Sanadi and associates (9) >40 years ago, accumulating evidence has suggested that FB plays an important role in the coupling of proton translocation to ATP synthesis during oxidative phosphorylation in animal mitochondria. Based on the N-terminal sequence of FB purified from bovine heart mitochondria (13), cDNAs encoding full-length human (2) and bovine (14) polypeptides have been reported. Search of sequence databases has identified an FB paralog in humans (2) and other animal species. Recombinant mature human and bovine FB polypeptides, comprised of 175 amino acid residues, have been purified from the soluble fraction of *E. coli* (2, 14) and were shown to be functionally active in reconstituting energy-driven reactions of oxidative phosphorylation (2, 8, 14). Recombinant bovine FB inhibits passive proton diffusion through bovine membrane sector F_o (15). A FB deletion mutant lacking Trp-2–Gly-3–Trp-4 from the mature amino acid sequence exhibited a decreased coupling activity (15). Cross-linking studies placed FB in proximity to the membrane sector F_o subunits *e* and *g* and the ADP/ATP carrier (15). Altogether, the available data suggest that FB facilitates energy-driven catalysis of ATP synthesis by blocking a proton leak through an alternative proton exit pathway, perhaps, within the membrane sector F_o.

We now report the high-resolution crystal structure of bovine mitochondrial FB. The structure reveals a globular N-terminal capping domain with a novel fold and an extended C-terminal domain composed of four leucine-rich repeats (LRRs). Although the LRR motif occurs in a variety of proteins (16, 17), its presence in a polypeptide associated with the matrix side of the mitochondrial inner membrane is unique. An α-helix at the N terminus provides structural evidence for a possible mode with which FB may bind to the surface of the mitochondrial inner membrane. The presence of a bound Mg^{2+} ion identifies FB as a metalloprotein. Phenylarsine oxide (PAO) and Cd^{2+}, two known inhibitors of the FB coupling activity, were found to bind Cys-71 and Cys-101, respectively, revealing the possible mode of inhibition of FB function by these ligands.

Results

Structure. We determined the crystal structure of WT bovine FB and the Gly-3–Glu mutant. This glycine-to-glutamate substitution occurs in the amino acid sequences of rat and mouse FB (14). The WT crystallized in the $C222_1$ space group with four identical molecules per asymmetric unit and diffracted to a maximum resolution of 2.9 Å. The Gly-3–Glu mutant formed crystals in the C2 space group with one molecule per asymmetric unit and diffracted to 0.96-Å resolution. The Cα positions of WT and mutant structures superimpose with rmsd between Cα of 0.57 Å between the two crystal forms. The summary of data collection and refinement statistics are recorded in Table 1.

The atomic-resolution structure of Gly-3–Glu mutant FB describes the coordinates of all of the 175 amino acid residues constituting the mature bovine FB. The structure reveals an oblong, oval-shaped molecule (Fig. 1) that folds into two domains: the N-terminal domain (residues 1–61) and the C-terminal LRR-containing domain (residues 62–175). The two domains are demarcated by a Lys-61–Ile-62 peptide bond, cleavage of which with trypsin in full-length recombinant FB releases the LRR domain as a stable proteolytic product (15).

Author contributions: J.K.L. and G.I.B. designed research; J.K.L. and G.I.B. performed research; J.K.L., G.I.B., and R.M.S. analyzed data; and J.K.L., G.I.B., and R.M.S. wrote the paper.

The authors declare no conflict of interest.

This article is a PNAS Direct Submission.

Freely available online through the PNAS open access option.

Data deposition: The atomic coordinates have been deposited in the Protein Data Bank, www.pdb.org (PDB ID codes 3DZE, 3E2J, 3E3Z, and 3E4G).

[‡]To whom correspondence maybe addressed. E-mail: gbelo@ucla.edu or stroud@msg.ucsf.edu.

Table 1. Data collection and refinement statistics

Crystal data	Native (Gly-3–Glu mutant)	Bromine	PAO	Cadmium	Native (WT)
Space group	*C*2	*C*2	*C*2	*C*2	$C222_1$
Unit cell, Å	$a = 107.5$	$a = 107.0$	$a = 106.1$	$a = 108.0$	$a = 99.6$
	$b = 50.0$	$b = 49.9$	$b = 49.7$	$b = 49.9$	$b = 133.9$
	$c = 36.9$	$c = 36.9$	$c = 36.9$	$c = 115.7$	$c = 115.7$
	$\beta = 109.4°$	$\beta = 109.4°$	$\beta = 108.8°$	$\beta = 109.6°$	
X-ray data collection statistics					
Wavelength, Å	1.0332	0.92011	0.97946	1.033	1.11
Resolution, Å	30–0.96	40–1.7	40–1.7	40–1.15	40–2.9
Total reflections	582,581	171,183	262,283	369,254	268,289
Unique reflections	95,951	37,171	19,212	62,187	16,810
Redundancy (last shell)	4.2 (1.6)	18.6 (7.9)	3.6 (3.3)	3.3 (1.5)	3.9 (3.1)
Completeness (last shell), %	100 (100)	93.0 (59.1)	95.51 (75.82)	93.3 (48.6)	95.9 (77.5)
R_{sym} , %	0.078	0.037 (0.24)	0.039	0.036	0.076
I/σ (last shell)	15.7 (2.0)	23.1 (2.82)	29.74 (9.8)	32.18 (1.8)	16.8 (1.78)
Crystallographic refinement statistics					
Resolution, Å	30–0.96	40.0–1.7	30–1.7	40–1.15	40.0–2.9
Reflections in working set	91,109	18,109	18,233	58,183	15,935
Reflections in test set (% of total)	4,829 (5)	967 (5)	978 (5)	3,104 (5)	841 (5)
R_{cryst}, %	14.3	16.1	14.1	12.9	23.6
R_{free}, %	16.4	19.8	18.8	15.5	32.9
rmsd bonds, Å	0.006	0.006	0.01	0.006	0.02
rmsd angles,°	1.06	0.976	1.15	1.06	1.74
Average *B* factors, Å^2	10.3	20.4	25.1	10.3	69.8
Phasing					
Resolution, Å		40–1.8			
Bromine sites		4			
Phasing figure of merit		0.66			

rmsd is the rmsd from ideal geometry. $R_{sym} = \Sigma_{hkl}\Sigma_i|I_{hkl,i} - \langle I_{hkl,i}\rangle|/\Sigma_{hkl}\Sigma_i|I_{hkl,i}|$, where $\langle I_{hkl,i}\rangle$ is the average intensity of the multiple hkl observations for symmetry-related reflections. $R_{cryst} = \Sigma||F_{obs}| - |F_{calc}||\Sigma|F_{obs}|$, where F_{obs} and F_{calc} are observed and calculated structure factors. R_{free} is calculated from a randomly chosen 5% or 10% of reflections, and R_{cryst} is calculated over the remaining reflections.

The presence of the LRR motif within FB was suggested earlier based on its amino acid sequence analysis (14).

The N-terminal domain is made up of three helices (α1–3) and one β-strand (β1) that runs antiparallel to the LRR motif β-strands. The β-strand from the N-terminal domain contributes to an extended concave β-sheet surface of the LRR domain and the metal binding site (see below). The amino acid content and location of helix α1, which is formed by residues 1–10 and includes four aromatic residues and four hydrophobic residues, suggests its possible role as a membrane anchor. Supporting this idea, a FB deletion mutant lacking the Trp-2–Gly-3–Trp-4 tripeptide exhibited a decreased coupling activity (15). Additionally, substitution of Trp-2 with a photoreactive unnatural amino acid *p*-benzoyl-L-phenylalanine yielded cross-links between FB and the membrane sector F_o subunits *e* and *g* and the ADP/ATP carrier (15). Tryptophan residues are often found at the termini of transmembrane helices, in proximity to the interface between the membrane and solvent. Here, the N-terminal aromatic residues Phe-1, Trp-2, and Trp-4, located at the tip of helix α1, could probably partition into the interfacial phase, facilitating attachment of the polypeptide to the membrane surface and determining the overall orientation of the polypeptide relative to the membrane plane.

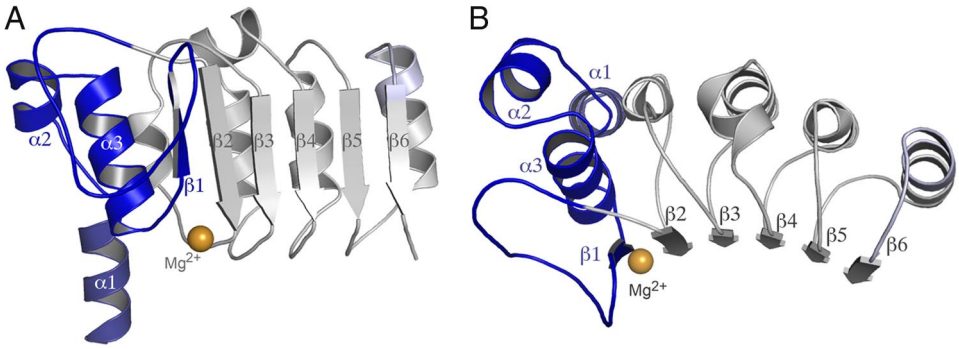

Fig. 1. Overall structure of bovine mitochondrial FB Gly-3–Glu mutant at 0.96-Å resolution. (*A*) The model includes all of the 175 amino acid residues of the mature bovine polypeptide. In slate is the N-terminal helix α1, and in blue is the remainder of the N-terminal domain, which includes the Mg^{2+} coordination site. In gray is the LRR domain, which contains four LRRs and the nuclear-export signal motif in human FB (highlighted in blue tint). FB is proposed to bind to the matrix side of the mitochondrial inner membrane in the shown orientation, with α1 helix dipping into the membrane interfacial phase. (*B*) View from the matrix side normal to the membrane, ≈90° rotated about the horizontal with respect to *A*.

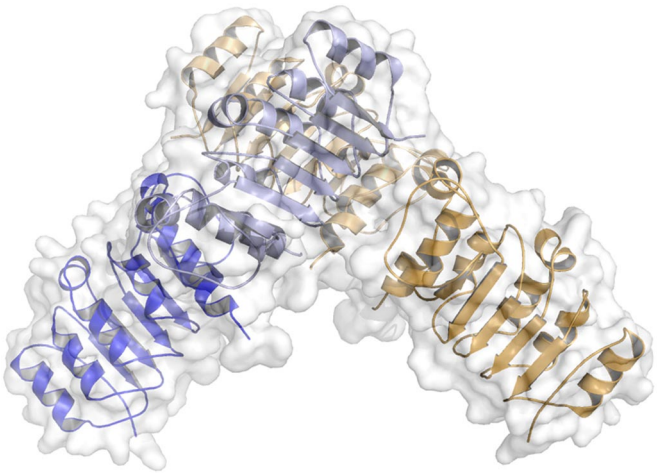

Fig. 2. A model of crystal structure of WT bovine FB refined at resolution of 2.9 Å. The tetramer is composed of a pair of dimers shown in blue/slate and orange/yellow-orange.

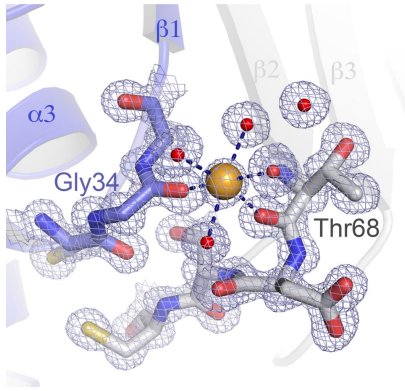

Fig. 3. Metal binding site in FB. The magnesium ion is coordinated by the carbonyl oxygens of Gly-34 and Thr-68 and four water molecules. No magnesium was added to the crystallization condition, which contains 1 mM EDTA, suggesting a high-affinity site for magnesium or other divalent metal *in vivo*. The electron density ($2\ F_O - F_C$) map is contoured at 1σ (blue).

The LRR domain of FB features the characteristic LRR motif of a concave solenoid shape that includes four tandem LRRs. The canonical LRR motif is comprised of a repeat of α/β fold with intervening loops (18), in which each repeating unit stacks to form a parallel β-sheet on one side and parallel α-helices on the other. The result of the tandem LRRs is a curved concave β-sheet, which usually functions as a ligand or protein binding surface (16, 19, 20). The N terminus of the LRR region of FB is capped by helix α3, a trend seen in many LRR domains in which a terminal helix blocks the hydrophobic core of the extended LRR solenoid. Residues 161–170, which comprise the nuclear export signal motif in human FB (21), form the top loop of the fourth LRR.

Bovine FB contains six cysteine residues, Cys-33, Cys-71, Cys-92, Cys-94, Cys-101, and Cys-123, of which two pairs, Cys-33/Cys-71 and Cys-94/Cys-123, could potentially form disulfide bridges (sulfur atoms at distances of 3.7 and 4.7 Å, respectively). When the recombinant protein was prepared in the presence of 2 mM DTT and 1 mM EDTA, no disulfide bridges were apparent in the structures. However, omitting the reducing agent and chelator during the purification led to crystals containing a single Cys-33–Cys-71 disulfide bond. Although no difference in Cα positions between the reduced and oxidized forms of the protein was observed, the binding affinity of oxidized polypeptide to FB-depleted mitochondrial membranes decreased by ≈3 fold, from K_d = 113 nM for the reduced protein to K_d = 352 nM for the oxidized protein (G.I.B., unpublished data).

The structure of the WT FB is a crescent-like assembly of two dimers, with residues from helix α1 and convex sides of two adjacent monomers contributing to the major contact points between two dimers (Fig. 2). Significantly, in the model depicted in Fig. 2, the overall orientation along the *y* axis of all four monomers constituting a tetramer is roughly the same, with four α1 helixes of each monomer pointing downward, thus establishing what could be considered as the top and bottom surfaces of the FB tetramer molecule. Within each dimer, two FB molecules are arranged in an opposite, head-to-head direction. The hydrophobic residues of helix α1 minimize their exposure to solvent by clustering with each other. At the dimer interface, residues Tyr-96, Ile-75, Met-73, and Glu-98 show the highest buried surface area. Previous biophysical studies, including analytical centrifugation, gel filtration, and cross-linking (22), and centrifugation in sucrose density gradient in the presence of a detergent (15), have demonstrated that FB undergoes reversible oligomerization in solution in a concentration-dependent manner (22). The importance of the α1 helix packing in FB oligomerization is highlighted by the fact that deletion of Trp-2–Gly-3–Trp-4 sequence increases the abundance of a monomer species in solution (15), and the Gly-3–Glu mutant crystallizes as a monomer. Cross-linking studies, however, reveal that the latter substitution does not prevent the formation of oligomeric species in solution (15). Whereas the total buried surface per each central monomer is ≈1,100 Å^2, the presence of the oligomers in solution suggests that the tetramer observed in the asymmetric unit of WT FB is physiologic and not caused by crystal packing. A cryo-electron microscopic analysis of the fragments of animal mitochondria has revealed dimers of the mitochondrial ATP synthase forming ribbons at the highly curved apexes of the mitochondrial cristae (23). This peculiar supramolecular organization of the mitochondrial ATP synthase was proposed to enhance the enzyme's performance under proton-limited conditions. The molecular dimensions of the FB tetramer, as revealed by its crystal structure, and the angle at which two FB dimers interact to form a tetramer, lead us to propose that *in vivo* a FB tetramer could assemble from the matrix-facing side at the curved apexes of the mitochondrial cristae within either an individual ATP synthase dimer or at the ATP synthase dimer–dimer interface. Such a location of FB within a specific set of aforementioned ATP synthase molecules could efficiently seal a proton leak that might be expected to occur at the interface formed between the angularly associated membrane sectors F_o of adjacent ATP synthase monomers.

Metal Binding Site. Among the novel features of FB revealed by the structure is the presence of a metal ion at the lower end of the β1–β2 strand pair in all of the crystals that were used for the data collection (Fig. 3). The atom is coordinated by the carbonyl oxygens of Gly-34, Thr-68, and four water molecules in an octahedral geometry. The octahedral coordination geometry of the atom, the electron density signal very similar to a water molecule, and bond lengths all suggest magnesium as the likely atom, and its presence identifies FB as a metalloprotein. Because FB was purified and crystallized in buffers that included 1 mM EDTA, the presence of the metal in the crystals suggests that it may be tightly bound. The bound magnesium could stabilize FB tertiary structure or provide an additional coordination site that facilitates interaction of FB with either its protein partner or a lipid headgroup at the mitochondrial membrane surface. The identity of a metal ion that could occupy this site in a membrane-bound FB *in vivo* is not known; a metal ion other than Mg^{2+}, such as Zn^{2+}, could be suggested. Indeed, a well-documented inhib-

BIOPHYSICS

itory effect of Zn^{2+} on proton pumping in cytochrome *c* oxidase has been described (24). It could be envisioned that side chains of Glu/Asp or His residues of a FB membrane-bound partner might become recruited to coordinate the metal, substituting for water molecules detected in the present structure (Fig. 3). Should such residues are found to alternatively contribute to a proton leakage pathway within membrane sector F_o, then a FB-bound Zn^{2+} might compete with protons for the same residues. This proposal could provide a plausible mechanistic explanation for the experimentally observed ability of FB to block proton leak (2, 8, 14). The discovery of Mg^{2+} bound by FB could also explain the requirement for high Mg^{2+} concentrations (15 mM) during preparation of tightly coupled bovine heart submitochondrial particles (25).

Inhibitors: PAO and Cadmium. PAO, which is known to bind preferentially to vicinal thiols, potently inhibits the coupling activity of FB (2, 12, 26). PAO is thought to react with vicinal cysteine residues by forming covalent bonds between its trivalent arsenic atom and the two sulfur atoms of the adjacent sulfhydryls. Another reaction mechanism entails the formation of single covalent bond between the arsenic atom and a cysteine sulfur and hydrogen bond between the arsenic atom and a water molecule. Two pairs of cysteine residues, Cys-33/Cys-71 and Cys-94/Cys-123, are potential targets for reacting with PAO. Structures of crystals soaked with PAO revealed the inhibitor arsenic atom forms covalent bonds only to the sulfur atom of Cys-71 and to a water molecule (Fig. 4 *A* and *B*).

The FB adduct with PAO showed no significant structural difference from that of free FB (rmsd = 0.11Å). Therefore, one can rule out conformational change as the basis behind the loss of the coupling activity observed in PAO-modified FB. Rather, the PAO molecule bound to Cys-71 is in close proximity to helix α1 and may interfere with the binding of helix α1 to the membrane. This conclusion derived from structural data is in contrast with that derived in earlier studies that found a lack of effect of modification with PAO on the binding of FB to the membrane (26).

Reaction of PAO with the second pair of vicinal cysteines, Cys-94 and Cys-123, was not observed, even at increased concentrations of the reagent. Residues Cys-94 and Cys-123Å are located within the interior of the first and second LRR, respectively, and are not readily accessible to solution. These residues could be even less accessible in the membrane-bound FB, and it is likely that PAO does not have adequate access to react with this pair of residues. Also, these cysteine sulfurs form hydrogen bonds to carbonyl oxygens of adjacent LRR repeat and form part of the network of interactions that stabilizes the stacking of these repeats. It cannot be excluded that reactivity of the remaining cysteines toward PAO could have been influenced by a particular experimental setup used in the present study. Among these, Cys-92 and Cys-101 are water-accessible and could potentially be expected to form adducts with PAO via a mechanism not unlike that described for Cys-71. The inability to detect the aforementioned adducts could be because incorporation of additional PAO molecules could have a destabilizing effect on FB structure, selecting for an adduct species with highest reactivity and stability under the experimental conditions. Additional studies using the protein chemistry approaches in conjunction with site-directed mutagenesis of specific cysteine residues are certainly required to reach a more definite conclusion regarding reactivity of the remaining sulfhydryls to PAO and mechanisms by which their modification could contribute to a loss of FB coupling activity.

Cadmium is also known to inhibit FB coupling activity (2, 12, 26). The crystal structure of a FB crystal soaked in a solution containing 10 mM Cd^{2+} reveals that the metal is a ligand for Cys-101 of the second LRR repeat (Fig. 4*C*). This is an unexpected finding because both Cd^{2+} and PAO were thought to react with the same pair of vicinal thiols (12).

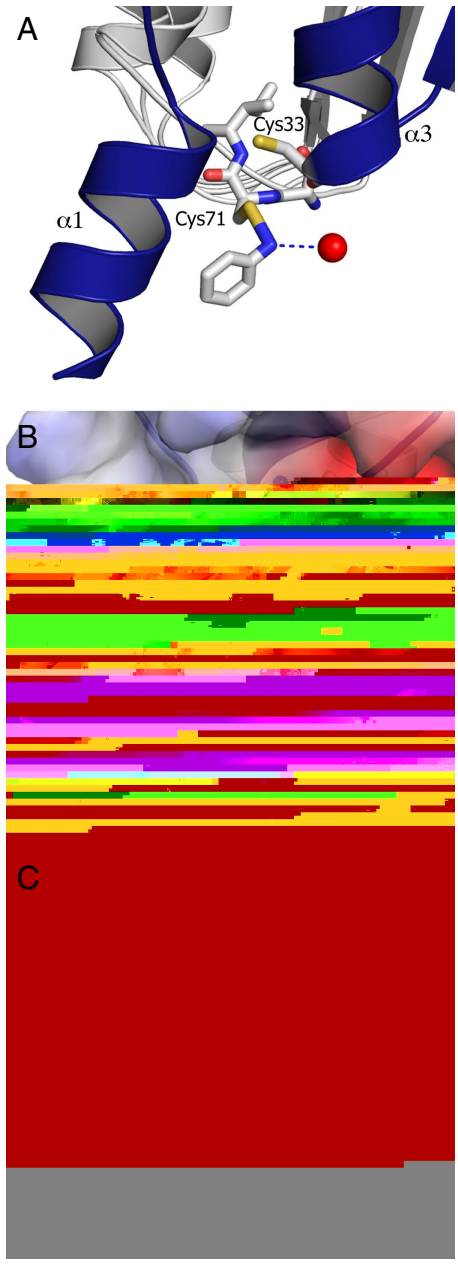

Fig. 4. Detailed view of the PAO and Cd^{2+} binding sites in FB. (*A*) PAO forms a covalent bond with the sulfur atom of Cys-71 via a dehydration reaction in which the hydroxide is released from PAO and the arsenic atom forms a covalent bond with the sulfur atom of Cys-71 and a hydrogen bond with a nearby water molecule. (*B*) Surface view of phenylarsine covalently bound to Cys-71 that shows the phenyl ring fitting into a hydrophobic pocket between helix α1 and the bottom surface of strand β1. (*C*) Cadmium binds to Cys-101 at the α-helical repeat region of the second LRR. The additional coordination is provided by three water molecules. The electron density ($2F_O - F_C$) map is contoured at 1σ (blue).

Discussion

The N terminus of bovine FB is a 10-residue α-helix (α1) that extends away from the main body of the molecule and is comprised of four hydrophobic (G3, L5, A7, V8), four aromatic (F1, W2, W4, F9), and two polar residues (N6, N10). This sequence forms an amphipathic helix that is completely aromatic/hydrophobic in the

first five residues and the two polar residues form a polar face near the C terminus of the helix. The amphipathic nature of this helix along with the position of helix α1 relative to the core of FB molecule suggests that it could dip into the interfacial membrane phase, positioning the remainder of the molecule in a lateral direction along the membrane surface. According to this interpretation, the loops connecting the C termini of the β-strands to the N termini of the α-helices of the LRRs are oriented along the membrane surface, unlike the LRR domain of Toll-like receptor 3 (27), in which the LRRs angle away from the membrane-spanning helix and no discrete interaction is possible between the protein and the membrane surface. This suggestion is reinforced by location of the Mg^{2+}-binding site, as well as Cys-71 and Cys-101 residues, which bind PAO and Cd^{2+}, respectively. These residues are all near the surface that could be considered as a membrane-associating side of the molecule, contributing to the interface between FB and either the protein or lipid components of the mitochondrial membrane. The LRR domain is probably required for a proper positioning of FB molecule at the membrane surface via the additional interactions either with membrane sector F_o subunits or phospholipid headgroups or both. Biochemical studies, however, demonstrate that on its own, the recombinantly expressed LRR domain of FB (residues 61–175) lacks the coupling activity of full-length polypeptide, at least in an ATP-driven proton-translocation assay (15). By contrast, mutational and cross-linking studies point to the important role of the proximal N-terminal residues, constituting helix α1, for the FB coupling mechanism (15). In agreement with a previous suggestion on the role of LRR motif (16), we therefore propose that the LRR domain of FB could function as a framework for protein–protein or protein–lipid interactions.

The mechanism of the Cd^{2+}-linked inhibition of the FB coupling activity could not be immediately discerned from the structure of Cd^{2+}-bound FB. Originally, Cd^{2+} was demonstrated to uncouple oxidative phosphorylation in rat liver mitochondria, which was prevented by dithiols (28). Subsequent studies have suggested FB as one of the targets of the metal within the mitochondrial inner membrane (9, 12). At present, it is not known whether in a membrane-bound FB, a metal ion, if any, is involved in coordinating Cys-101. The binding of exogenous Cd^{2+} to a normally metal-free site could perturb protein–protein interaction between FB and its putative membrane-bound partner. The existence of additional targets for Cd besides FB cannot be ignored as well, to explain uncoupling effects of the metal in mitochondria documented in earlier studies.

In bovine heart mitochondria, FB is found in association with the mitochondrial inner membrane (2). It is readily displaced into solution during disruption of bovine heart mitochondria with ultrasound in a buffer of pH $\approx$8.8 containing 0.6 mM EDTA. The weak binding affinity of FB with the mitochondrial inner membrane has caused a controversy, stemming primarily from the fact that the protein was not found in a preparation of bovine heart mitochondrial F_1F_o ATPase (29). The ease with which FB is lost during extraction and purification procedures can account for the fact that ATP–$^{32}P_i$ exchange activity of most preparations of the enzyme from mammalian sources is either low (2) or can be further stimulated by exogenously added polypeptide (8). As was proposed earlier (2), a reversible change in a redox status of a FB vicinal dithiol, linked to a change in the intramitochondrial redox state, could be used to regulate the extent of proton leak through F_o, such that a transient mild uncoupling could occur after a reversible vicinal disulfide formation caused by excessive production of reactive oxygen species. This mechanism could allow the polypeptide to act as a redox sensor and maintain the proton-motive force below a damaging threshold level within mitochondria. The x-ray structure of FB presented here has now revealed that most plausible candidates for such vicinal thiols are residues Cys-33 and Cys-71.

In the present study we have reported the atomic-resolution structure of bovine heart mitochondrial coupling FB. The structure provides a precise description of the molecular architecture of the polypeptide, identifies cysteine residues targeted by inhibitors of its coupling activity, ands suggests a possible mode in which the polypeptide could interact with the mitochondrial inner membrane. The high-resolution structure also provides a framework for future structure–function studies aimed at the mechanism of the FB coupling activity and its putative role in oxidative phosphorylation in animal mitochondria.

Materials and Methods

Expression and Purification. Recombinant bovine FB (both WT and Gly-3–Glu mutant) was expressed and purified as described (14). FB-NusA fusion polypeptide was purified in the native conditions from soluble fraction of BL21(DE3)pLysS strain of *E. coli* transformed with pET43-bFB-2–1 vector (14). The purification procedure included affinity enrichment of the fusion polypeptide on Ni-NTA agarose, followed by size-sieving and ion-exchange chromatographies. After overnight cleavage of FB-NusA with thrombin, FB was finally purified on DEAE-Sepharose FF. The purified polypeptide was concentrated up to 15–20 mg/ml by using an Amicon Ultra centrifugal concentrator and stored in aliquots at -80°C. Extraction and all of the purification steps were performed at 4°C, and all of the buffers included 2 mM DTT and 1 mM EDTA. Recombinant bovine FB used for crystallization contains a Ser residue at its N terminus, followed by a complete 175-residue sequence (14).

The binding affinities of reduced and oxidizied FB, which harbors Cys-33–Cys-71 disulfide bond, were calculated from titration experiments that monitored the enhancement of steady-state levels of ΔpH in FB-depleted membrane vesicles (14), generated via ATP-driven proton pumping activity, after reconstitution of the vesicles with increased concentrations of exogeneously added FB (unpublished work).

Crystallization and Data Collection. Initial screening of crystallization conditions of WT FB (at $\approx$20 mg/ml) was carried out by using the microfluidic TOPAZ screening chip (Fluidigm) and the hanging drop method. A condition producing crystals in a TOPAZ chip was further optimized by the hanging drop method using 2-μl amounts of drops at 4°C and 22°C. Best crystals formed in $\approx$3 days, matured to $<$100 μm along the longest edge, and diffracted to maximum resolution of 2.8 Å.

Crystals of the Gly-3–Glu mutant were grown at 4°C by the vapor diffusion method using a 1:1 mixture of FB at $\approx$20 mg/ml concentration and a crystallization condition containing 50% polypropylene glycol 400 (PEG400), with 100 mM Tris adjusted to pH 7.4–8.0. Crystals of the mutant appeared in $\approx$3 days and matured to their maximum size of $>$500 μm in $\approx$1 week. The microseeding method was used with good results to improve nucleation and size of the crystals.

For phasing, mature crystals were soaked in 1 M NaBr solution (1 M NaBr, 50% PPG400, 100 mM Tris, pH 7.5) for 30–120 s (30) and flash-frozen in liquid N_2. SAD data at the Br edge were collected from cryo-cooled (100 K) crystals at beamline 8.3.1 of the Advanced Light Source (Berkeley, CA) to resolution of 1.7 Å (Table 1). Native data sets for the mutant diffracted to maximum resolution of 0.96-Å resolution. Data of the PAO-bound crystals were collected at beamline 9–1 of the Stanford Synchrotron Radiation Laboratory (Stanford, CA). The cadmium data set was collected at beamline 8.3.1 of the Advanced Light Source. The data sets were indexed and reduced by using the program HKL2000 (31).

Structure Determination and Refinement. The initial solution of the structure was found by using the Phenix system (32). Four bromine sites were located for phasing followed by solvent flattening. This model was refined at 1.8-Å resolution with REFMAC5 (33) and later refined by using native data to 0.96 Å. A random sampling (5%) of data was omitted from refinement for R_{free} calculations. The refined model includes every residue in the protein, including the residual N-terminal serine residue left over from the cleavage of the affinity tag. The native data set of the mutant was complete to maximum resolution of 0.96 Å. The PAO- and cadmium-bound structures were refined at 1.7 and 1.15 Å, respectively. The WT FB is refined at 2.9-Å resolution. The figures were prepared with PyMOL (34).

ACKNOWLEDGMENTS. We thank Andy May of Fluidigm Corporation for help with crystallization screening and visualization with the TOPAZ system and J. Finer-Moore for discussion and critical reading of the manuscript. Support for this work was provided by National Institutes of Health Grants 5U54GM074929 (to R.M.S.) and GM066085 (to G.I.B.), and National Institutes of Health Roadmap Center Grant P50 GM073210 (to R.M.S.).

1. Hatefi Y (1985) The mitochondrial electron transport and oxidative phosphorylation system. *Annu Rev Biochem* 54:1015–1069.
2. Belogrudov GI, Hatefi Y (2002) Factor B and the mitochondrial ATP synthase complex. *J Biol Chem* 277:6097–6103.
3. Senior AE, Nadanaciva S, Weber J (2002) The molecular mechanism of ATP synthesis by F_1F_o-ATP synthase. *Biochim Biophys Acta* 1553:188–211.
4. Ko YH, Delannoy M, Hullihen J, Chiu W, Pedersen PL (2003) Mitochondrial ATP synthasome. Cristae-enriched membranes and a multiwell detergent screening assay yield dispersed single complexes containing the ATP synthase and carriers for P_i and ADP/ATP. *J Biol Chem* 278:12305–12309.
5. Chen C, *et al.* (2004) Mitochondrial ATP synthasome: Three-dimensional structure by electron microscopy of the ATP synthase in complex formation with carriers for P_i and ADP/ATP. *J Biol Chem* 279:31761–31768.
6. Abrahams JP, Leslie AGW, Lutter R, Walker JE (1994) Structure at 2.8-Å resolution of F_1-ATPase from bovine heart mitochondria. *Nature* 370:621–628.
7. Stock D, Leslie AGW, Walker JE (1999) Molecular architecture of the rotary motor in ATP synthase. *Science* 286:1700–1705.
8. Belogrudov GI (2002) Factor B is essential for ATP synthesis by mitochondria. *Arch Biochem Biophys* 406:271–274.
9. Lam KW, Warshaw JB, Sanadi DR (1967) The mechanism of oxidative phosphorylation. XIV. Purification and properties of a second energy-transfer factor. *Arch Biochem Biophys* 119:477–484.
10. Joshi S, Hughes JB, Shaikh F, Sanadi DR (1979) On the role of coupling factor B in the mitochondrial P_i-ATP exchange reaction. *J Biol Chem* 254:10145–10152.
11. Joshi S, Sanadi DR (1979) Purification of coupling factor B. *Methods Enzymol* 55:384–391.
12. Sanadi DR (1982) Mitochondrial coupling factor B. Properties and role in ATP synthesis. *Biochim Biophys Acta* 683:39–56.
13. Kantham L, *et al.* (1990) Amino-terminal amino acid sequence of beef heart mitochondrial coupling factor B. *FEBS Lett* 277:105–108.
14. Belogrudov GI (2006) Bovine factor B: Cloning, expression, and characterization. *Arch Biochem Biophys* 451:68–78.
15. Belogrudov GI (2008) The proximal N-terminal amino acid residues are required for the coupling activity of the bovine heart mitochondrial factor B. *Arch Biochem Biophys* 473:76–87.
16. Kobe B, Kajava AV (2001) The leucine-rich repeat as a protein recognition motif. *Curr Opin Struct Biol* 11:725–732.
17. McEwan PA, Scott PG, Bishop PN, Bella J (2006) Structural correlations in the family of small leucine-rich repeat proteins and proteoglycans. *J Struct Biol* 155:294–305.
18. Kobe B, Deisenhofer J (1993) Crystal structure of porcine ribonuclease inhibitor, a protein with leucine-rich repeats. *Nature* 366:751–756.
19. Kobe B, Deisenhofer J (1995) A structural basis of the interactions between leucine-rich repeats and protein ligands. *Nature* 374:183–186.
20. Marino M, Braun L, Cossart P, Ghosh P (2000) A framework for interpreting the leucine-rich repeats of the Listeria internalins. *Proc Natl Acad Sci USA* 97:8784–8788.
21. Belogrudov GI (2007) A 24-residue presequence localizes human factor B to mitochondria. *Arch Biochem Biophys* 461:95–103.
22. Belogrudov GI, Schirf V, Demeler B (2006) Reversible self-association of recombinant bovine factor B. *Biochim Biophys Acta* 1764:1741–1749.
23. Strauss M, Hofhaus G, Schroder RR, Kuhlbrandt W (2008) Dimer ribbons of ATP synthase shape the inner mitrochondrial membrane. *EMBO J* 27:1154–1160.
24. Qin L, *et al.* (2007) Crystallographic location and mutational analysis of Zn and Cd inhibitory sites and role of lipidic carboxylates in rescuing proton path mutants in cytochrome *c* oxidase. *Biochemistry* 46:6239–6248.
25. Lee CP (1979) Tightly coupled beef heart submitochondrial particles. *Methods Enzymol* 55:105–112.
26. Joshi S, Hughes JB (1981) Inhibition of coupling factor B activity by cadmium ion, arsenite-2, 3-dimercaptopropanol, and phenylarsine oxide, and preferential reactivation by dithiols. *J Biol Chem* 256:11112–11116.
27. Choe J, Kelker MS, Wilson IA (2005) Crystal structure of human toll-like receptor 3 (TRL3) ectodomain. *Science* 309:581–585.
28. Jacobs EE, Jacob M, Sanadi DR, Bradley L (1956) Uncoupling of oxidative phosphorylation by cadmium ion. *J Biol Chem* 223:147–156.
29. Walker JE, Lutter R, Dupuis A, Runswick MJ (1991) Identification of the subunits of F_1Fo-ATPase from bovine heart mitochondria. *Biochemistry* 30:5369–5378.
30. Dauter Z, Dauter M, Rajashankar KR (2000) Novel approach to phasing proteins: Derivatization by short cryo-soaking with halides. *Acta Crystallogr D* 56:232–237.
31. Otwinowski Z, Minor W (1997) Processing of x-ray diffraction data collected in oscillaltion mode. *Methods Enzymol* 276:307–326.
32. Adams PD, *et al.* (2002) PHENIX: Building new software for automated crystallographic structure determination. *Acta Crystallogr D* 58:1948–1954.
33. Murshudov GN, Vagin AA, Dodson EJ (1997) Refinement of macromolecular structures by the maximum-likelihood method. *Acta Crystallogr D* 53:240–255.
34. DeLano WL (2002) The PyMOL molecular graphics system (DeLano Scientific, San Carlos, CA).